Morphological Investigations of Single Levitated $H_2SO_4/NH_3/H_2O$ Aerosol Particles during Deliquescence/Efflorescence Experiments

Christina A. Colberg,* Ulrich K. Krieger, and Thomas Peter

Institute for Atmospheric and Climate Science, Swiss Federal Institute of Technology, Hönggerberg HPP, 8093 Zurich, Switzerland

Received: November 27, 2003; In Final Form: January 26, 2004

In an electrodynamic particle trap, experiments with single levitated $H_2SO_4/NH_3/H_2O$ aerosol particles have been performed under atmospheric conditions. Four analytical methods provide independent information on the aerosol composition and structure (measurements of Mie scattering, Raman scattering, scattering fluctuations, and of mass). The morphology of the aerosol particles and the water uptake and drying behavior are investigated including the determination of deliquescence and efflorescence relative humidities. In general, the thermodynamic data derived from our measurements are in good agreement with previous work. The observed solid phase is mostly letovicite $[(NH_4)_3H(SO_4)_2]$ and sometimes ammonium sulfate $[(NH_4)_2SO_4]$, whereas ammonium bisulfate $[(NH_4)HSO_4]$ does not nucleate at temperatures between 260 and 270 K despite supersaturation over periods of up to 1 day. This underlines the atmospheric importance of letovicite, which has been ignored in most previous studies concentrating on ammonium sulfate. When the stoichiometry of the aqueous solution in the droplets is chosen as neither that of ammonium sulfate nor letovicite, the particles forming after efflorescence are mixed-phase particles (solid/liquid), representing the usual case in the natural atmosphere. Upon crystallization these mixed-phase particles reveal a range of different morphologies with a tendency to form complex crystalline structures with embedded liquid cavities, but there is no evidence for the occurrence of crystalline material surrounded by the remaining liquid. This liquid possibly resides in grain boundaries or triple junctions between single crystals or in small pores and shows little mobility upon extensive drying, unless the shell-like surrounding solid cracks.

1. Introduction

Because of their scattering and absorbing properties, atmospheric aerosol particles affect the radiative balance of the Earth. Besides this direct climatic effect, aerosol particles contribute also indirectly as cloud precursors to the terrestrial radiation budget. Neither the direct nor the indirect effects are quantitatively well characterized, leading to large uncertainties in the global mean radiative forcing caused by aerosol particles, which may counteract the forcing by greenhouse gases to a large degree.[1] In particular, the exact role of aerosols in the formation mechanisms of cirrus clouds is poorly understood, although about 30% of the Earth is covered with cirrus clouds.[1] The net radiative effect of a cirrus cloud may be either to warm or cool the Earth, depending on the altitude (and hence temperature) and optical density of the cloud (the so-called greenhouse-versus-albedo effects).[2] It is important to understand the processes that control the cloudwater content, the crystal shape, and the crystal size distribution, because the warming/cooling balance depends strongly on such properties.[3] Consequently, microphysical understanding of the mechanisms associated with cirrus cloud formation is required to obtain reliable estimates of this budget. For example, microphysical knowledge is needed to assess the effects of aviation in the context of increases in cirrus cloud cover.[1,4] Experimental laboratory work can be applied to investigate microphysical aerosol processes, helping to provide a basis for our understanding and for parametrizations applied in cloud models and numerical weather prediction models.[5]

The physical state of aerosol particles is of substantial interest in particular with regard to the microphysical aerosol behavior. The process in which dry solid crystals stay dry upon humidification but take up water spontaneously above a certain relative humidity (RH) to form an aqueous solution is called deliquescence, and the corresponding RH value thermodynamically required for this to happen is called the deliquescence relative humidity (DRH). The inverse process of solidification is called efflorescence, which is, in contrast to deliquescence, not thermodynamically determined but a kinetic nucleation phenomenon requiring supersaturation. The RH value typically required for solidification is called the efflorescence relative humidity (ERH). The fact that ERH is not equal to the DRH (but is often considerably lower) is called the deliquescence/efflorescence hysteresis. Recently, the first systematic global calculation of the physical state of atmospherically relevant $H_2SO_4/NH_3/H_2O$ aerosol particles that takes this hysteresis fully into account has been performed in a Lagrangian trajectory study.[6]

Because in atmospheric particles the stoichiometry of the droplets is unlikely to correspond precisely to the crystallizing solid, usually a liquid remains upon crystallization. Therefore, by far most of the atmospheric aerosol particles are not expected to become totally dry and solid but rather to form a mixed phase, containing a solid and a remaining liquid. The morphologies of these particles may be complex and diverse. Following Weis and Ewing,[7] principal morphological structures are illustrated in Figure 1, which displays a single crystal (I), an agglomerate of single crystals or a polycrystalline solid (II), a polycrystalline

* Corresponding author: E-mail: christina.colberg@env.ethz.ch.

10.1021/jp037628r CCC: $27.50
Published on Web 03/11/2004

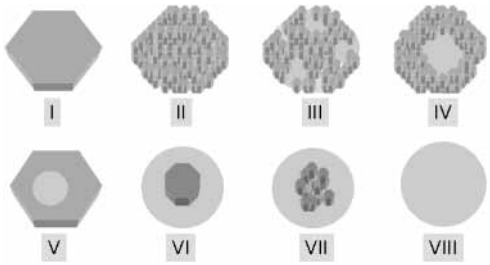

Figure 1. Possible structures of aerosol particles.[7] Morphological differences are displayed: (I) single crystal; (II) agglomerate of single crystals, respectively, a polycrystalline solid; (III) polycrystalline material with several open but liquid-filled cavities; (IV) solid polycrystalline shell with embedded liquid; (V) solid single-crystalline shell with embedded liquid; (VI) single crystal with surrounding liquid; (VII) polycrystalline solid with surrounding liquid; (VIII) liquid aerosol particle. It must be pointed out that the polycrystalline materials might contain different solids.

material with several open cavities filled with liquid (III), a solid polycrystalline shell with embedded liquid (IV), a solid single-crystalline shell with embedded liquid (V), a single crystal with surrounding liquid (VI), a polycrystalline solid with surrounding liquid (VII), and a totally liquid aerosol particle (VIII). Work using electron microscopy[8−10] indicates that atmospheric aerosol particles indeed occur as complex aggregates with all kinds of different morphologies. Mostly this is influenced by the fact that atmospheric aerosol particles may have complex compositions; however, there is evidence that complex morphologies exist even in aerosol particles consisting of only two species. An IR spectroscopic flow tube study[7] of solid NaCl aerosol particles effloresced from aqueous solutions shows that they still contain water. The liquid is most likely present in pockets or trapped by a solid shell. Shell formation has also been observed in similar electrodynamic balance experiments[11] during the crystallization of NaCl solution droplets.

Besides radiative effects, the morphology of aerosol particles is also of interest with regard to heterogeneous chemistry. Although heterogeneous chemistry involving liquid aerosol particles is conceptually understood and a well-established framework for parametrizations does exist,[12] the same does not hold true for heterogeneous reactions on solid or mixed-phase aerosol surfaces (most prominently ice surfaces). In general, heterogeneous chemistry on solid atmospheric particles can be influenced by liquid films on these particles. Thereby diffusion kinetics and solubility are influenced by the sample morphology, such as porosity, polycrystallinity, and impurities at grain boundaries or in veins or triple junctions (i.e., the locations where three grains meet).

Ammonium, nitrate, and sulfate have been known for a long time to be components of the atmospheric aerosol, and their importance is corroborated by recent studies.[13−17] Moreover, theoretical studies show that ammoniated sulfate aerosols may be important for cirrus cloud formation.[18,19] Of course, tropospheric aerosol particles are not just a mixture of $NH_3/H_2SO_4/HNO_3/H_2O$ but may also contain sea salt, organic compounds, elemental carbon, and,in traces, practically any element.[20] Their composition varies widely with geographical location and altitude.[21] Recent aerosol time-of-flight mass spectrometric measurements of single atmospheric aerosol particles[20,22,23] highlight the importance of organics and elemental carbon besides water soluble inorganic compounds. However, a large fraction especially of the middle and upper tropospheric aerosols can be described approximately as quaternary mixtures of the $NH_3/H_2SO_4/HNO_3/H_2O$ system.[24] By means of a thermodynamic model, the so-called AIM (aerosol inorganic model) model,

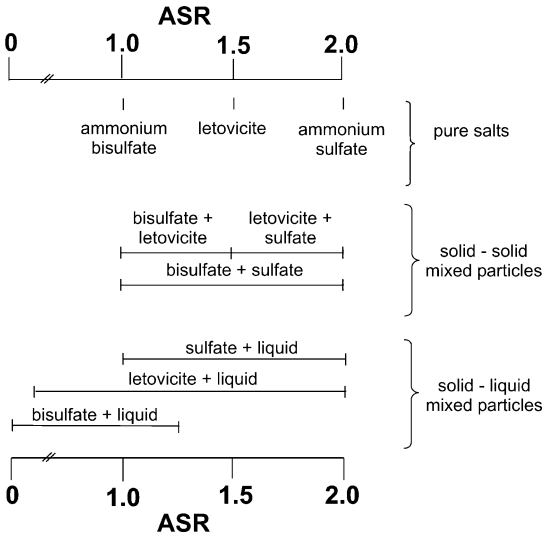

Figure 2. Thermodynamically expected pure solid particles, their internal mixtures, and mixtures of one of the solids together with a remaining liquid at 260 K within the $H_2SO_4/NH_3/H_2O$ system (Courtesy of K. Carslaw, University of Leeds, U.K.). The possibility of sulfuric acid hydrate formation is not considered because it is known that these do not crystallize.[48]

Clegg et al.[25] determined the composition and phases of the aerosol at a given RH and temperature of the $NH_3/H_2SO_4/HNO_3/H_2O$ system at atmospheric temperatures. Because there is a lack of low-temperature data of the $NH_3/H_2SO_4/HNO_3/H_2O$ system, the AIM model of Clegg et al.[25] is mainly based on experimental data obtained at room temperature.

In a next step of simplification one may note that there is little HNO_3 in sulfate aerosol particles in the upper troposphere, largely because of the rather low mixing ratios of HNO_3.[26] Field measurements of continental aerosol particles show besides many other particles (containing, e.g., organics) also almost pure ammoniated sulfate particles.[9] Therefore, the present work investigates the $H_2SO_4/NH_3/H_2O$ system as a reasonable first approximation. However, even the ternary system is complex and difficult to investigate, restricting the laboratory data to subsets of the system and to special temperature/pressure conditions. Phase transitions in the binary systems H_2SO_4/H_2O[27] and $(NH_4)_2SO_4/H_2O$[28,29] have been studied extensively. Single-particle experiments at room temperatures have been performed with $(NH_4)_2SO_4/H_2O$[30,31] and with $NH_3/H_2SO_4/H_2O$[32,33] aerosol particles. In addition, a recent flow tube study[34] investigated the crystallization behavior of $NH_3/H_2SO_4/HNO_3/H_2O$ aerosol particles at room temperature.

Data obtained with bulk samples of the NH_4HSO_4/H_2O system[35−37] are in good agreement with the AIM model.[25] Yet, single-particle levitation measurements of the NH_4HSO_4/H_2O system[38] and the $(NH_4)_2SO_4/H_2O$ system[39] disagree with the model.[25] A number of studies[40−45] deal with the supercooling properties of $(NH_4)_2SO_4/H_2O$ droplets, particularly with respect to homogeneous ice nucleation. Heterogeneous nucleation experiments of internally mixed $(NH_4)_2SO_4/H_2O$ droplets and mineral contaminations[46,47] show that these contaminations may increase the efflorescence relative humidity significantly.

Figure 2 shows the thermodynamic compositions of solid and partially solid particles within the $H_2SO_4/NH_3/H_2O$ system as a function of the ammonia-to-sulfate ratio (ASR). Conceivable solids are NH_4HSO_4 (ammonium bisulfate, ASR = 1), $(NH_4)_3H(SO_4)_2$ (letovicite, ASR = 1.5), and $(NH_4)_2SO_4$ (ammonium sulfate, ASR = 2). Sulfuric acid hydrates are not expected to form because their small nucleation probabilities

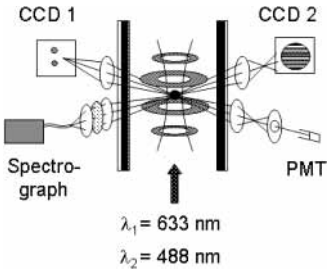

Figure 3. Experimental setup of the single-particle levitation apparatus.

prevent their crystallization.[48] Even aerosol particles consisting of only two components (e.g., $NaCl/H_2O$) may crystallize in complex morphologies.[7,11] The numerous combinations of phases in the $H_2SO_4/NH_3/H_2O$ system displayed in Figure 2 are expected to show complex morphologies as well.

In this paper, we use the technique of single-particle levitation to study the $H_2SO_4/NH_3/H_2O$ aerosol system. The morphology, DRH, and ERH, as well as the water uptake and loss are studied by storing particles with different ASR in an electrodynamic trap.

2. Experimental Section

The experimental setup used in our experiments is described in detail elsewhere.[49] A schematic representation of the main features of the apparatus is shown in Figure 3. An electrically charged particle (typically $2-20$ μm in diameter) is balanced in an electrodynamic trap.[50] The balance is hosted within a three-wall glass chamber with a cooling agent flowing between the inner walls and an insulation vacuum between the outer walls. The temperature can be varied between 330 and 160 K with a stability better than 100 mK and an accuracy of $\pm$ 0.5 K. A constant flow (typically 30 sccm) of a N_2/H_2O mixture with a controlled H_2O partial pressure is pumped continuously through the chamber at a constant total pressure adjustable between 200 and 1000 mbar. During an experiment, the temperature is kept constant and the relative humidity within the chamber is increased or decreased continuously by changing the N_2/H_2O ratio, using automatic mass flow controllers. A single-particle generator (Hewlett-Packard 51633A ink jet cartridge) is used to inject one liquid particle with a fixed ammonia-to-sulfate ratio (ASR).

Four independent analytical tools provide information on the particle: (i) mass from dc voltage, (ii) radius from Mie phase function analysis, (iii) composition from Raman spectroscopy, and (iv) particle shape and morphology from intensity fluctuation measurements. These techniques are applied as follows.

(i) Two collinear laser beams illuminate the levitated particle from below (HeNe: 632.8 nm, 3 mW. Ar^+: 488.0 nm, 400 mW). We use the video image of the particle on CCD 1 and an automatic feedback loop to adjust the dc voltage for compensating the gravitational force.[51] A change in dc voltage is a direct measurement for the particles mass change and, if the gas phase contains only water vapor, its concentration change.

(ii) The fringe pattern (measured with CCD 2) of the elastically scattered light of both lasers is compared with Mie theory to deduce the radius (and refractive index) of a liquid particle.[52] After a liquid-to-solid transition occurs, the fringe pattern loses its regular, periodic structure (thus no meaningful radius values can be obtained for solid particles, see Figure 4d).

(iii) We apply Raman spectroscopy, using the Ar^+-laser as an excitation source in a 90° scattering geometry without an analyzing polarizer, to identify solid phases of the particles. Two holographic notch filters are used to reject the elastically scattered light of both lasers, and an optical fiber is employed to deliver the Raman-shifted light to a 150 mm spectrograph with a slow scan back-illuminated CCD (charge-coupled device) array detector. Because Raman reference spectra are needed for comparison, we used bulk samples which are held at an adjustable temperature and also measured in a 90° scattering geometry with an identical detection setup as in our levitation apparatus. For ammonium sulfate and ammonium bisulfate crystals we used commercial samples (Aldrich, purity > 99.999%). The letovicite crystals were generated from a

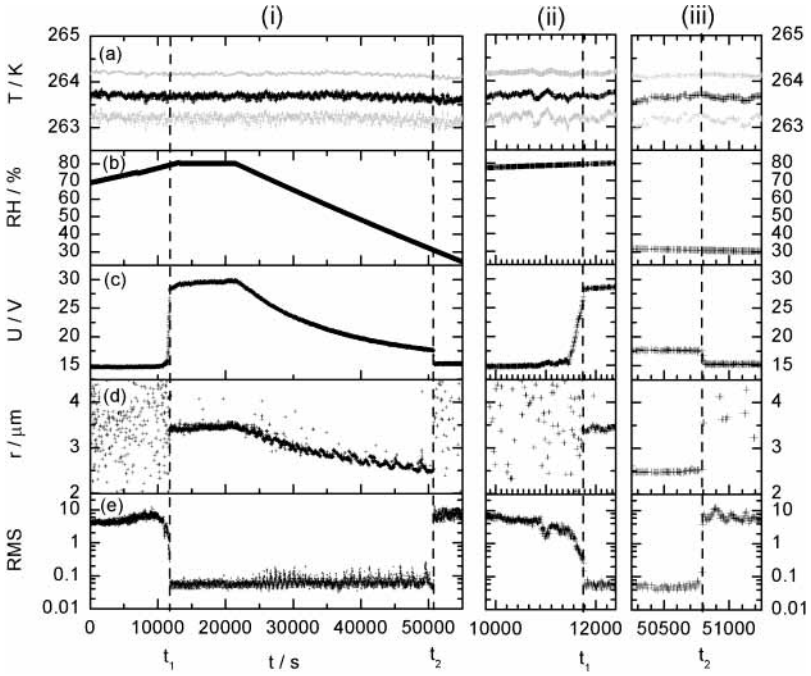

Figure 4. Typical set of raw data for a deliquescence/efflorescence experiment with an $(NH_4)_2SO_4/H_2O$ aerosol particle. Vertical panel (i) shows the complete data set, whereas panels (ii) and (iii) zoom in on the deliquescence and the efflorescence points, respectively. The horizontal panels show (a) temperature, (b) RH, (c) U_{dc} voltage, (d) particle radius, and (e) rms (root mean square deviation) of the scattering intensity fluctuation.

saturated, equimolar solution of the aforementioned solids according to established crystallization methods.[53]

(iv) Finally, we use a photomultiplier with a relatively small conical detection angle (approximately 0.2° half-angle) to measure the scattering intensity at 90° to the incident beam and feed this signal to an analogue lock-in amplifier to measure the intensity fluctuations, that is, the root mean square deviation from the intensity mean. Because of its symmetry, a homogeneous spherical particle will show a constant scattering intensity and hence a very small fluctuation amplitude. A nonspherical particle will scatter light with different intensity in the detection angle depending on its orientation relative to the incoming laser beam. (All particles perform Brownian rotational motion in an electrodynamic balance.) We have used these intensity fluctuation amplitudes previously to characterize liquid microdroplets with a single solid inclusion.[54,55] There, we confirmed the power law dependence of the fluctuation amplitudes with the area of the inclusions predicted by a modeling study.[56] The same study showed that the intensity fluctuations can be used to measure the concentration of very small inclusions in a microdroplet. In the following we will use this to identify the occurrence of phase transitions and to characterize the morphology of complex aerosol particles.

Within the $H_2SO_4/NH_3/H_2O$ system, aqueous solutions of the solids $(NH_4)_2SO_4$ (ASR = 2), $(NH_4)_3H(SO_4)_2$ (ASR = 1.5), and NH_4HSO_4 (ASR = 1) were examined. Moreover, aerosol particles with ASR values of 0.5, 0.3, and 0 (pure H_2SO_4) were investigated. For each ASR, 1.25 wt % solutions were prepared by adding deionized water to stoichiometrically appropriately mixed $(NH_4)_2SO_4$ and NH_4HSO_4 crystals (Aldrich, purity > 99.999%) and a 2.5 wt % solution of H_2SO_4 (Aldrich, purity > 99.9%), respectively. After injection, the $(NH_4)_xH_y(SO_4)_z/H_2O$ droplets equilibrate in a controlled atmosphere under atmospheric conditions.

Deliquescence and efflorescence experiments were performed by increasing or decreasing RH at constant temperature. Initially, completely solid single-component particles deliquesce in a clear step (at the DRH). In contrast, mixed-phase particles take up water gradually so that the unambiguous identification of the DRH is less clear. For such particles, the DRH is given by the RH above which the particle is completely liquid. Thus, the intensity fluctuation measurements are the ideal tool to determine the DRH because the fluctuations are highly sensitive to the presence of even small solid cores in a liquid droplet.

Figure 4 shows the time-dependent raw data of a typical experiment with an aerosol particle with precise $(NH_4)_2SO_4/H_2O$ stoichiometry. Panel a shows the temperature as measured with sensors inside the trap, which is practically constant in this case. The gray curves show the temperatures of the coldest and warmest locations in the chamber. The black curve is the averaged temperature, which is used for comparison with the AIM model. Panel b shows the RH calculated from the flows measured by the automatic mass flow controllers; panel c shows the dc voltage compensating the gravitational force; panel d shows the particle radius, which is calculated with Mie phase function analysis[52] for the two different laser wavelengths (λ = 633 nm and λ = 488 nm). For aspherical, that is, solid or mixed-phase particles, Mie phase function analysis provides random values (see scatter) with very distinct transitions from spherical to aspherical and back. Panel e shows the root mean square deviation (rms) of the scattering intensity (intensity fluctuation data in (d)), which qualitatively characterizes the deviation from a perfect sphere and therefore the morphology of an aerosol particle. Small values (rms < 0.05) correspond to spherical droplets, whereas large values (rms > 1) correspond to very aspherical particles. During this particular experiment a solid $(NH_4)_2SO_4$ aerosol particle is humidified. It deliquesces at $t_1 \approx 11\,770$ s (DRH = 79%) and takes up further water until the RH is kept constant at RH = 80%. A mass change of 5% already occurs at an RH 0.5% lower than the DRH. The fact that a slight water uptake is detected before the actual DRH is discussed in detail in section 3.2. In the experiment the RH was subsequently decreased ($t \approx 21\,500$ s) and water evaporates continuously. Once the RH < DRH (t > 22 700), the particle starts being supersaturated and the hysteresis region is reached. Eventually, the crystal effloresces ($t_2 \approx 50\,800$ s; ERH = 30.2%) and loses all its remaining water spontaneously. Further decrease in RH does not result in any further changes of dc voltage or rms values. The maximum absolute errors in the temperature, radius, and U_{dc} are $\Delta T = \pm 0.35$ K, $\Delta r = \pm 0.25$ μm, and $\Delta U_{dc} = \pm 0.5$ V, respectively. The errors of the RH determination are ΔRH = ± 2.5% for RH < 80% and ΔRH = ± 5% for RH > 80%.

Depending on the ASR and therefore the chemical composition of the investigated aerosol particle, different solids form upon crystallization within the $H_2SO_4/NH_3/H_2O$ system. The deliquescence pathways may be different for $(NH_4)_2SO_4$, $(NH_4)_3H(SO_4)_2$, and NH_4HSO_4 particles. As long as they are purely crystalline without concomitant liquid, the crystals absorb water spontaneously and deliquesce very rapidly at the DRH. This behavior is observed during the $(NH_4)_2SO_4$ deliquescence cycle displayed in Figure 5, corresponding to structures (I) and (II) of Figure 1. However, as soon as the aerosol particles are mixed and the liquid is in any contact with the gas phase (structures (III), (VI), and (VII) of Figure 1) the deliquescence behavior differs. As the RH increases the remaining liquid takes up water and starts to dissolve the crystal. This leads to a continuous deliquescence process until the DRH is reached (the RH above which the solid particle is fully dissolved). An example for this kind of process would be an $(NH_4)_3H(SO_4)_2$ particle, which grew from an NH_4HSO_4 solution.

Therefore, the deliquescence behavior is more complex if mixed solid particles with an ASR not corresponding to one of the crystals (ASR = 2, 1.5, or 1) are investigated. Multiple deliquescence steps are expected in these cases.

3. Results and Discussion

We performed experiments with 33 different particles running multiple deliquescence/efflorescence cycles: we accomplished 6 experiments for ASR = 2; 3 experiments for ASR = 1.5; 14 experiments for ASR = 1; 2 experiments for ASR = 0.5; 2 experiments for ASR = 0.31; and 6 experiments for ASR = 0.

3.1. Thermodynamic Investigation. Figure 5 shows deliquescence/efflorescence cycles for $(NH_4)_2SO_4/H_2O$ (ASR = 2) and $(NH_4)_3H(SO_4)_2/H_2O$ (ASR = 1.5) aerosol particles at T = 263.5 K. The gray lines represent AIM model results[25] for the deliquescence and efflorescence characteristics of $(NH_4)_2SO_4$ and $(NH_4)_3H(SO_4)_2$ crystals, respectively. The large gray circles show droplet concentrations as determined from the radius data of the Mie phase function analysis and the small black circles show droplet concentrations as derived from the change in particle mass from the U_{dc} measurement. In these cases crystals formed which correspond to the investigated ASR ($(NH_4)_2SO_4$ and $(NH_4)_3H(SO_4)_2$, respectively). The crystals were identified by Raman spectroscopy.[57] The dry particles contained no liquid, and a spontaneous deliquescence was observed. The radius as well as the mass data agree within the experimental error with the AIM model.[25]

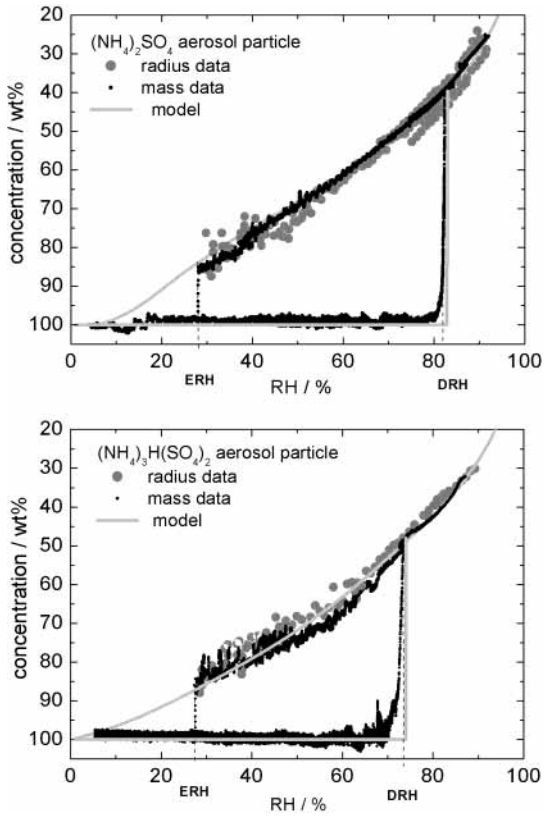

Figure 5. Deliquescence/efflorescence cycles for $(NH_4)_2SO_4/H_2O$ (ASR = 2) and $(NH_4)_3H(SO_4)_2/H_2O$ (ASR = 1.5) aerosol particles at T = 263.5 K. To obtain the concentration scale the experimental data are normalized to the concentration of a liquid aerosol calculated by the AIM model[25] at the RH values right after the deliquescence is observed (here, 82.2% and 73.2%, respectively). Gray lines: AIM model.[25] Gray circles: droplet concentrations obtained from the radius data (Mie phase function analysis). Small black circles: concentrations derived from the mass data (dc measurements). A mass increase of 5% occurs already at RH = DRH − 0.8% before reaching the deliquescence point of the $(NH_4)_2SO_4/H_2O$ system and at RH = DRH − 1.9% in the $(NH_4)_3H(SO_4)_2/H_2O$ system.

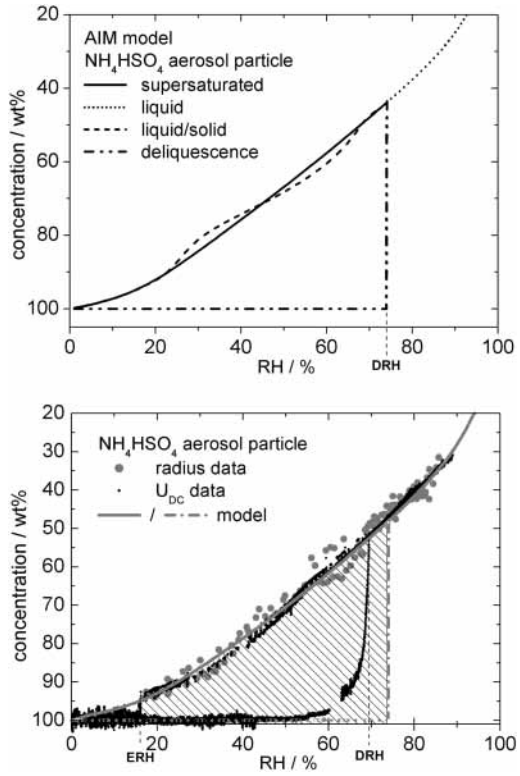

Figure 6. (a) AIM model results for an NH_4HSO_4/H_2O (ASR = 1) aerosol particle at T = 260 K. Solid line: particle assumed to remain liquid. Dashed line: solid $(NH_4)_3H(SO_4)_2$ assumed to precipitate surrounded by remaining liquid. Dashed-dotted line: a solid $(NH_4)_3H(SO_4)_2$ shell assumed to enclose the remaining liquid. Dotted line: liquid droplet beyond the DRH. (b) Experimental deliquescence/efflorescence cycle data for an NH_4HSO_4/H_2O (ASR = 1) aerosol particle at T = 260.5 K. To obtain the concentration scale the experimental data are normalized to the concentration of a liquid aerosol calculated by the AIM model[25] at the RH values right after the deliquescence is observed (here, 69.4% RH). Gray lines: AIM model.[25] Large gray circles: droplet concentrations obtained from radius data. Small black circles: particle concentrations derived from mass data. Hatched area: region in which different deliquescences of $(NH_4)_3H(SO_4)_2$ in the NH_4HSO_4/H_2O are expected (compare text). A mass increase of 5% occurs already at RH = DRH − 6.2% before reaching the deliquescence point of the NH_4HSO_4/H_2O system.

However, the deliquescence behavior is more complex for NH_4HSO_4/H_2O aerosol particles. If $(NH_4)_3H(SO_4)_2$ crystallizes from a NH_4HSO_4/H_2O solution, which is predicted by the AIM model,[25] a liquid remains. For such mixed-phase aerosol particles different morphologies are conceivable (structures III, IV, V, VI, and VII in Figure 1). These potential morphologies could be classified into two groups: (α) the remaining liquid surrounds the solid or (β) the remaining liquid is shielded by the surrounding solid. Assuming (α) that the crystal is surrounded by the liquid (structures VI and VII in Figure 1), thermodynamic considerations result in continuous dissolution of the crystal when the RH is increased. The concentration characteristics for the humidifying/deliquescence (solid and remaining liquid) and drying/efflorescence (supersaturated solution) processes are expected to be different. This is due to the fact that upon crystallization the composition of the remaining liquid changes compared to the supersaturated solution. This yields to a change of the water activity and therefore water vapor pressure of the solution. However, according to the AIM model[25] this effect is rather small and the concentration characteristics are nearly identical for the humidifying and drying cycles. Both processes are plotted in Figure 6a as a dashed black line for the mixed-phase particle and as a solid gray line for the supersaturated particle.

Assuming (β) that the solid $(NH_4)_3H(SO_4)_2$ encloses the remaining liquid and therefore shields it from the ambient gas phase (structures IV or V in Figure 1), the crystalline particle would behave as if $(NH_4)_3H(SO_4)_2$ had formed from a $(NH_4)_3H(SO_4)_2/H_2O$ solution (ASR = 1.5, DRH = 73%). This is plotted in Figure 6a as the dashed-dotted gray line.

However, the deliquescence pathway of aerosol particles with ASR = 1 shows a behavior unexpected from these thermodynamic considerations. As in Figure 5, the deliquescence and efflorescence cycles for ASR = 1 are illustrated in Figure 6b. Again for the drying process (efflorescence) the radius and mass data agree within the experimental error with the AIM model,[25] whereas the deliquescence data show a large deviation from the model curves described in Figure 6a.

Therefore, we studied the deliquescence behavior of $H_2SO_4/NH_3/H_2O$ aerosol particles with ASR = 1 in more detail. With the Raman spectra shown in Figure 7, the solid particle is identified as $(NH_4)_3H(SO_4)_2$, Therefore, a liquid remains after the crystallization, and morphology classes α and β need to be considered (see above). We see a distinct difference between the humidifying and drying processes which disagrees with the described scenario α. Moreover, we find a DRH substantially

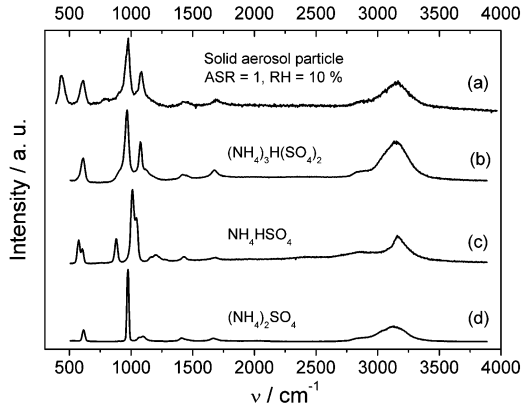

Figure 7. (a) Raman spectrum of a solid aerosol particle originating from a solution droplet with ASR = 1 and $r \approx 10$ μm at RH = 10%. (b−d) Raman spectra of bulk reference samples: (b) letovicite, (c) ammonium bisulfate, (d) ammonium sulfate. Comparison allows one to identify the solid aerosol particle as letovicite. For all spectra, the $\nu_1(SO_4^{2-})$ bands (the $\nu_1(HSO_4^-)$ band for NH_4HSO_4) are normalized. The detailed band assignment in the Raman spectra and a description of further reference and aerosol spectra will be given elsewhere.[57] All spectra are taken at $T = 260$ K.

TABLE 1: Measured ERH and DRH Values from Single-Aerosol Particle Experiments in the Electrodynamic Particle Trap[a]

ASR	ERH/%homogeneous	DRH /%	T /K	solid phase
2	30.8	81	263.5	$(NH_4)_2SO_4$
	28.5	81.5	260	$(NH_4)_2SO_4$
1.5	27.5	72.8	263.5	$(NH_4)_3H(SO_4)_2$
1	16	70−75	270	$(NH_4)_3H(SO_4)_2$
	16	70−76	264	$(NH_4)_3H(SO_4)_2$
	15	66−73	260	$(NH_4)_3H(SO_4)_2$
0.5	<1		263.5	no nucleation
0.31	<1		263.5	no nucleation
0	<1		258−290	no nucleation

[a] Each ERH and DRH value is an average of up to seven experiments. Measurements are performed at constant temperatures. Errors are ± 2.5% in RH. For ASR = 1, due to morphological differences of the crystals after efflorescence, DRH is not one constant value, but intervals are specified.

lower than that expected by the model. We do not see the behavior of scenario β as if $(NH_4)_3H(SO_4)_2$ had formed from a $(NH_4)_3H(SO_4)_2/H_2O$ solution (ASR = 1.5, DRH = 73%). Figure 6b shows that the real deliquescence behavior falls between the two extreme cases. This region is illustrated in Figure 6 as the hatched area. At this point it needs to be mentioned that only one observed deliquescence pathway is displayed in Figure 6b. The morphological differences of the investigated crystals in 26 deliquescence and efflorescence experiments with 14 individual NH_4HSO_4/H_2O aerosol particles result in a large variety of deliquescence pathways, indicating different morphologies. This interpretation is fully supported by the light-scattering data, which give direct evidence of the asphericity of the mixed-phase particles (see below in section 3.2.).

To summarize all our data the ERH and DRH values are shown in Table 1. The identification of the solid phases is performed by means of Raman spectroscopy. Efflorescence of solid NH_4HSO_4 is not observed in the electrodynamic particle trap in the given temperature range on the time scale of days (our longest experiments took 7 days). For ASR = 1, Table 1 gives a DRH range within deliquescences were observed. This is due to morphological differences of the investigated solids. Supersaturated droplets with ASRs of 0.5, 0.31, and 0 do not crystallize at all. Within the investigated temperature interval ($T = 260-270$ K) the values show no systematic temperature dependence. For ASR = 1 the variation in DRH is caused by the different morphologies of the crystals rather than by the different temperatures (as supported by the light-scattering measurement). However, the humidifying and drying characteristics for these experiments are in overall good agreement with the AIM model.[25]

Table 2 draws a comparison of our measurements with the available literature data of the $H_2SO_4/NH_3/H_2O$ system. The limited low-temperature ERH and DRH data available in the literature are restricted to the $(NH_4)_2SO_4/H_2O$ system (ASR = 2).[40,41] Taking into account the scattering and the error bars of these measurements,[40,41] their ERH data and our measurements are in good agreement. The fact that our values are at the lower bound of all values shows that we probably do not face the problem of heterogeneous nucleation, in particular because our scatter of ERH in different experiments is small. For the $(NH_4)_3H(SO_4)_2/H_2O$ system (ASR = 1.5) a comparison is not possible due to the lack of data. Data for the NH_4HSO_4/H_2O system (ASR = 1) is contradictory at first. Tang and Munkelwitz[33] observe between 5% and 22% RH NH_4HSO_4 crystallization at room temperature. Because of the scatter of their data, we assume that they detected heterogeneous nucleation. The crystallization we observe for ASR = 1 and $T = 260$ K is in contradiction to a flow tube study,[58] where crystallization was not observed for temperatures between 298 and 238 K. This might be due to residence times in the flow reactor of approximately 30 s, which might be too short to allow nucleation and crystallization to be observed. Also, the spectroscopic detection of crystallization is based on changes in the water band of the aerosol. This detection suffers if the aerosol is very dry, that is, it loses only marginal water during efflorescence. In contrast to these observations we propose that $(NH_4)_3H(SO_4)_2$ indeed forms through homogeneous nucleation at ERH = 16% ± 2.5%, since we identified it during 18 independent efflorescence cycles as the crystallization product. This is supported by the observation that we have obviously no problem in avoiding heterogeneous nucleation in our electrodynamic particle trap, as both $(NH_4)_2SO_4$[11,49] and NaCl[54] nucleate exactly at the accepted homogeneous ERH values, which are reported in the literature.[24]

3.2. Morphological Investigation. The deliquescence behavior of solid-containing particles of the NH_4HSO_4/H_2O (ASR = 1) system for different aerosol particles as well as for repeating deliquescences with one specific particle is diverse and surprisingly complex. Deliquescences of $(NH_4)_3H(SO_4)_2$ in the NH_4HSO_4/H_2O system are observed in an interval of 66% < RH < 76%. Additionally, a three-step deliquescence process is observed occasionally and is explained in detail in elsewhere.[59] The features of each deliquescence process are different. We characterize it by the amount of water uptake before the deliquescence, the change of the spherical properties during the whole deliquescence cycle, and by the DRH value itself. This is definitely not an artifact of the instrument because such differences do not depend on the rate of changing RH (dRH/dt) and are not observed in other systems, for example, the $(NH_4)_3H(SO_4)_2/H_2O$ and $(NH_4)_2SO_4/H_2O$ systems. Moreover, it is obvious that the different water uptake characteristics are connected to the fact that the aerosol particle is only partially solid and a liquid remains.

As illustrated in Figure 6a, two extreme cases are theoretically conceivable: (α) The crystalline $(NH_4)_3H(SO_4)_2$ is surrounded by the remaining liquid. The aerosol particle behaves similarly

TABLE 2: Comparison of Measurements of This Work with Available ERH and DRH Data of the $H_2SO_4/NH_3/H_2O$ System[a]

ASR	ERH/%	DRH/%	*T* /K	reference	method	solid phase
2	38.8 ± 6.2		234	40	FTS	$(NH_4)_2SO_4$
	42 ± 6		238	41	FTS	
	36.5 ± 6.2		244	40	FTS	
	36.2 ± 6.2		249	40	FTS	
	35.3 ± 6.2		253	40	FTS	
	42 ± 4		253	41	FTS	
		83 ± 4	254	41	FTS	
		82.3 ± 2	258	40	FTS	
	28.5 ± 2.5	81.5	260	this study	EDB	
	32.9 ± 2.5	82.6 ± 2	263	40	FTS	
		82 ± 3	263	41	FTS	
	30.8 ± 2.5	81	263.5	this study	EDB	
	32.8 ± 2.5		269	40	FTS	
	30.5 ± 2.5	81.1 ± 1.5	273	40	FTS	
	37 ± 3	82 ± 2	273	41	FTS	
		81 ± 2	283	41	FTS	
		79.7 ± 1.5	284	[40]	FTS	
	48	81	293	67, 68	EDB	
	31.8 ± 2.5		293.5	40	FTS	
	32.5 ± 2.5	79 ± 1.5	295	40	FTS	
	36	79.5	298	31	EDB	
	35	80	298	32	EDB	
	33 ± 2	79 ± 1	298	41	FTS	
	27 ± 2	79 ± 2	298	46	FTS	
	27 ± 2	79 ± 1	298	63	FTS	
1.5	27.5 ± 2.5	72.8 ± 2.5	263.5	this study	EDB	$(NH_4)_3H(SO_4)_2$
	35−44	69	298	31	EDB	
	31	71	298	32	EDB	
1	16 ± 2.5	66−76 ± 2.5	260−270	this study	EDB	$(NH_4)_3H(SO_4)_2$
	no nucleation		238−298	58	FTS	
	5−22	40	298	31	EDB	NH_4HSO_4
	no nucleation		298	63	FTS	

[a] EDB: electrodynamic balance. FTS: flow tube study.

as a supersaturated liquid. The water uptake is then rather continuous as calculated by the AIM model.[25] (β) The crystalline $(NH_4)_3H(SO_4)_2$ encloses the remaining liquid and therefore shields it from the ambient gas phase. The crystal would behave as if $(NH_4)_3H(SO_4)_2$ had formed from a $(NH_4)_3H(SO_4)_2/H_2O$ solution. The deliquescence and therefore the water uptake is spontaneous and takes place at the value for an $(NH_4)_3H(SO_4)_2$ crystal (ASR = 1.5) corresponding to a DRH of 73%.

However, a whole variety of deliquescence pathways have been observed. This is illustrated on the basis of three examples in Figure 8. The most extreme cases, which were observed during all experiments, are shown in panels 1 and 3, respectively, whereas panel 2 represents a case which could be described as a mixture of both. In all three cases the observed solid is $(NH_4)_3H(SO_4)_2$, which is verified by Raman spectroscopy. Normalized mass data (left *y*-axis) are plotted as black solid circles, and rms deviation of the intensity (right *y*-axis) is plotted as black crosses as a function of RH. The particle's dry mass is normalized to 1. Whenever the remaining liquid is trapped by the crystal during the nucleation process, water cannot evaporate and the remaining liquid is not in equilibrium with the coexisting crystal. At the beginning of a deliquescence cycle the particle mass is therefore occasionally larger than the dry mass (panels 1 and 2).

The deliquescence characteristic in panel 1 is the steepest deliquescence step which was measured in the NH_4HSO_4/H_2O (ASR = 1) system. Neither does the particle mass increase significantly nor does the particle become more spherical, as seen from the change in the fluctuation data, before the deliquescence at DRH = 71% (recall that the DRH of pure letovicite would be 73%). This, and the fact that the particle mass is 15% larger than the dry mass at the beginning of this deliquescence cycle, leads to the conclusion that in this case the crystalline $(NH_4)_3H(SO_4)_2$ encloses the remaining liquid nearly completely. The liquid is shielded from the ambient gas phase, and the crystal deliquesces like the pure salt $(NH_4)_3H(SO_4)_2$.

The deliquescence characteristic in panel 3 is the most continuous deliquescence which was measured in the NH_4HSO_4/H_2O (ASR = 1) system. The particle mass increases significantly, and the particle becomes clearly more spherical before the deliquescence at DRH = 68%. A 5% mass increase is observed already at 37.4% in RH before the DRH. The particle mass at the beginning of a deliquescence cycle is just slightly larger (2%) than the dry mass, which shows that the remaining liquid is equilibrated. However, the water uptake characteristic does not correspond to the AIM model,[25] which predicts a more continuous and less abrupt water uptake. Taking into account these findings, we assume that the crystalline $(NH_4)_3H(SO_4)_2$ shields the remaining liquid partially from the ambient gas phase. The small amount of remaining liquid which interacts with the gas phase provides the water uptake prior to deliquescence. The morphology of the solid-containing aerosol particle could be explained as an inclusion particle with embedded liquid cavities, for example, the liquid could be located between grain boundaries of single crystals or at pores with concave surfaces, rather than by a remaining liquid, which is totally surrounded by the crystal. This is strengthened by the fact that the Raman spectra shows the features of solid $(NH_4)_3H(SO_4)_2$.

The deliquescence characteristic in panel 2 represents a case which could be described as a mixture of the behaviors displayed in panels 1 and 3. Although the particle mass does not increase significantly, the particle becomes clearly more spherical before the deliquescence at DRH = 69%. A 5% mass change is

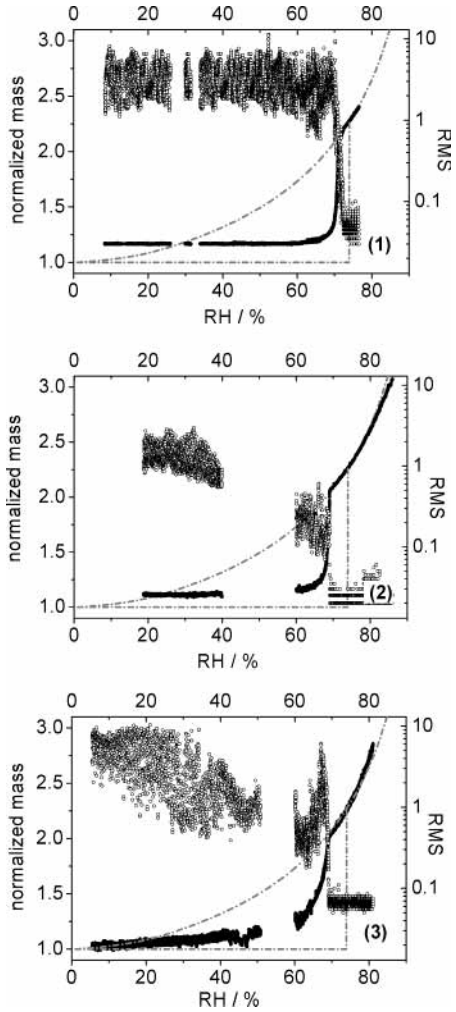

Figure 8. Different deliquescence pathways for the NH_4HSO_4/H_2O (ASR = 1) system. Black solid line: normalized mass data (left *y*-axis, starting from approximately 1). Black open circles: rms deviation of the intensity fluctuations (right *y*-axis, starting between 1 and 10). Gray dashed-dotted lines: AIM model.[25] The experimental mass data are normalized to the concentration of a liquid aerosol calculated by the AIM model[25] at the RH values right after the deliquescence is observed. A mass increase of 5% occurs already at RH = DRH − 4.4% in the particle in panel 1, at RH = DRH − 8.8% in the particle in panel 2, and at RH = DRH − 37.4% in the particle in panel 3. Data gaps are caused by technical reasons, e.g., recording Raman spectra.

observed 8.8% in RH before the DRH. At the beginning of the deliquescence cycle the particle mass exceeds the dry mass by 11%; this shows that in this case the crystalline $(NH_4)_3H(SO_4)_2$ encloses large parts of the remaining liquid. The liquid is shielded mostly from the ambient gas phase. However, some water uptake takes place, which results in a more spherical shape of the solid-containing aerosol particle before deliquescence, although the water uptake cannot be detected with a mass increase. This supports the finding that only a small part of the remaining liquid interacts with the ambient gas phase. This accounts for the water uptake prior to deliquescence, which is detected by the intensity fluctuation method. Again, the morphology of the solid-containing aerosol particle could be explained as inclusion particles with embedded liquid cavities, for example, the liquid could be located between grain boundaries of single crystals or at pores with concave surfaces.

The relative position of the DRH values and the relative values of the particle masses at the beginning of the deliquescence cycle are self-consistent. The more the remaining liquid interacts with the ambient gas phase, the smaller the observed DRH values and the particle masses are at the beginning of the deliquescence cycle.

These three examples show the variety of deliquescence pathways of crystalline $(NH_4)_3H(SO_4)_2$ with a remaining liquid formed out of an NH_4HSO_4/H_2O solution. There might be hybrids of the two proposed extreme structures with the tendency that inclusion particles with embedded liquid cavities are being formed. Of course these differences and the actual observed deliquescence characteristics cannot be predicted by thermodynamics alone.

The experiments performed during this study show that, in the ternary $H_2SO_4/NH_3/H_2O$ system, preferentially polycrystalline solids with several open and liquid-filled cavities (structure III in Figure 1) or solids with a polycrystalline shell with an embedded liquid (structure IV in Figure 1) are being formed. Hybrids of these two structures are also being observed. The reverse case, namely, that the crystal is totally surrounded by the remaining liquid (structures VI and VII in Figure 1), is not observed in any of the experiments.

Finally, two cases should be distinguished.

(i) The stoichiometry of the formed solid does not correspond to the ASR of the liquid droplet, and therefore, a liquid remains after crystallization. In natural aerosol particles this will almost always be the significant process. As explained above, the results of this study show that during the crystallization process the remaining liquid is trapped in the crystal. The liquid is either totally shielded (structure IV in Figure 1) or stored in several open cavities, which means that, for example, the liquid could be located between grain boundaries of single crystals or at pores with concave surfaces (structure III in Figure 1). The exact morphology, that is, the degree of how much the remaining liquid is shielded by the solid, differs not only from aerosol particle to aerosol particle but also from nucleation process to nucleation process. Moreover, the amount of liquid and therefore the partitioning between liquid and solid differs. Depending on the shielding degree water uptake can take place prior to deliquescence as characterized in Figure 8.

(ii) The stoichiometry of the formed solid corresponds to the ASR of the liquid droplet and therefore crystallizes totally. This case is atmospherically by far not as relevant as the above one but of high microphysical interest. A detailed inspection of the presented deliquescence curves in Figure 5 shows that approximately 2−3% in RH before the actual DRH a slight water uptake is being observed. Quantitatively speaking, this means that for the $(NH_4)_2SO_4$ aerosol particle the 5% mass increase is completed 0.8% and for the $(NH_4)_3H(SO_4)_2$ aerosol particle the 5% mass increase is completed 1.9% in RH before the DRH is reached. We call this predeliquescence, and its reason is most likely that small amounts of water are trapped during the nucleation process. As discussed above also, here the liquid could be located between grain boundaries of single crystals or at pores with concave surfaces. This predeliquescence is the object of another study. Such predeliquescence has been also observed in TDMA investigations.[60,61]

The occurrence of structures III and IV of Figure 1 are in accordance with literature results. Pure solid ammoniated sulfate particles, 0.1−1 μm in size, which are collected at a continental German site and analyzed by high-resolution scanning electron microscopy, tend to form agglomerates of primary ammoniated sulfate particles.[9] In a theoretical study[62] where the morphological control of particles generated from the evaporation of solution droplets is investigated, it is proposed that structure IV of Figure 1 is most likely to occur, because water evaporation

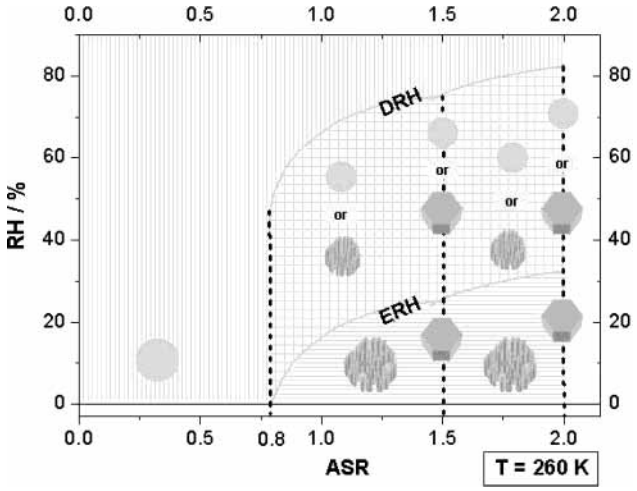

Figure 9. Schematic of possible physical states and morphologies of $H_2SO_4/NH_3/H_2O$ aerosol particles as a function of ASR and RH (at $T = 260$ K, whereas the temperature dependency is only small). DRH curve: AIM model[25] confirmed by our experimental data. ERH curve: calculated by subtracting a constant 50% RH from the DRH curve. This procedure[6] is in good agreement with our experimental data. Vertical shading: purely liquid droplets. Horizontal shading: Purely solid single-component or two-component particles. Checkered: Hysteresis region with either completely or partially solid or liquid particles, depending on the direction from which the hysteresis region was entered. (Note: ammonium bisulfate is not shown because homogeneous efflorescence did not occur in the experiments and is expected to be unlikely. The solid phase for $0.8 < \text{ASR} \lesssim 1.8$ is most likely letovicite. For $\text{ASR} \gtrsim 1.8$ ammonium sulfate is expected.)

generates a concentration profile with a higher concentration at the surface. Therefore, nucleation primarily starts at the surface and a solid shell could trap the remaining liquid. Laboratory experiments of NaCl in an electrodynamic balance[11] indicate the process of shell formation. Two FTIR spectroscopic flow tube experiments[7,63] of submicrometer solid NaCl particles (mean diameter: $d = 400$ nm) prove[63] that for RH < 4% a small amount of water is embedded in the crystals, which is rather physically trapped than adsorbed. Weis and Ewing[7] confirm this result and report that for RH < 50% an unexpected high amount of water is observed in the crystals. They suggest that water is trapped during the crystallization process and that the water is present in either open or shielded pockets. This results in similar structures like structures III and IV of Figure 1. Scanning electron photomicrographs[8] display that sea salt particles which are nucleated from seawater form hollow crystals, independent of whether they are from laboratory experiments or from samples of real particles in the field.

This arguments lead to the scheme of physical states and morphologies in Figure 9 if only homogeneous crystallization is considered. For ASR < 0.8 only liquid aerosol particles are expected because a homogeneous efflorescence point does not exist. Because of the hysteresis effect, the physical state of aerosol particles depends for ERH < RH < DRH on the direction from which this hysteresis region was entered.[6] Controlled by this hysteresis for ASR=1.5 and ASR=2, pure solids of letovicite and ammonium sulfate, respectively, or liquid droplets are anticipated. For all other ASR regions ($0.8 < \text{ASR} < 1.5$ and $1.5 < \text{ASR} < 2$) solids with a remaining liquid or liquid droplets, also depending on the RH, are expected. The morphologies of these particles are complex, and a tendency to shield the remaining liquid is being observed.

4. Conclusions and Atmospheric Implications

In general the thermodynamic data, DRH values and characteristics of water uptake and release, measured in the present work are in good agreement with the AIM model[25] as well as with other experimental data. Beyond thermodynamic data also kinetic aspects like ERH values and morphological properties were determined in the present study. The observed solid phases are letovicite and ammonium sulfate, which often exist as mixed-phase (solid/liquid) particles. These mixed particles were found to crystallize in different morphologies, which differ not only from particle to particle but also from nucleation to nucleation in deliquescence/efflorescence cycles of the same particle. The mixed-phase particles tend to form liquid inclusions, that is, the remaining liquid appears to be shielded against the gas phase. For example, the liquid could be located between grain boundaries or in veins or pores with concave surfaces.

These results should be applicable to the atmospheric $H_2SO_4/NH_3/H_2O$ aerosol particles. Often, however, the $H_2SO_4/NH_3/H_2O$ solution will also contain other species, such as organics, and it is not known at present how this will affect the morphological behavior of aerosols. Moreover, it needs to be taken into account that the aerosol particles investigated are typically between 2 and 20 μm in size, whereas atmospheric particles are substantially smaller.

For purely liquid droplets the water uptake and release characteristics, which are parametrized by the AIM model[25] and confirmed with our measurements, can be integrated into global radiation models or cloud-resolving models.

With the presented homogeneous ERH values the hysteresis region is determined as well. However, the water uptake characteristics of mixed-phase particles containing letovicite are influenced by the morphology. To parametrize the morphology-dependent water uptake characteristics, further systematic laboratory studies are needed. The breakup of shells surrounding a liquid would be of particular interest. In addition, field measurements, which explicitly analyze the morphology of the collected aerosol particles, would be desirable.

Although heterogeneous nuclei occur quite frequently in the atmosphere, their influence on atmospheric nucleation processes is still uncertain. However, a study[64] which investigated the heterogeneous freezing of aqueous particles with solid ammoniated sulfate nuclei suggests that the heterogeneous freezing temperature depends on the morphology of the solid. Therefore, further laboratory experiments are needed to improve our knowledge about the potential role of letovicite acting as a CCN during cirrus cloud formation.

Heterogeneous chemistry involving fully liquid aerosol particles is well understood conceptually.[12] However, the same does not hold true for heterogeneous reactions on solid aerosol surfaces or ice surfaces. In these cases, diffusion kinetics and solubility are influenced by the sample morphology, such as polycrystallinity, impurities at grain boundaries or at the junctions where three grains meet, and porosity. For instance, heterogeneous chemistry on solid NaCl particles can be influenced by liquid films on these particles.[65] Therefore, the influence of morphology on heterogeneous reactions of gaseous species with solid surfaces, in particular letovicite, should be studied in more detail. Concentration profiles at the surface of aerosol particles might be of interest as well. Ion-enhanced interactions with gases at aqueous interfaces may play a more generalized and important role in the chemistry of concentrated inorganic salt solutions than was previously recognized.[66]

Concerning climatic issues the question is how mixed-phase aerosol particles and the different morphological structures

influence radiative forcing. The effect of these particles on the scattering properties of visible light and therefore the direct aerosol effect has not been discussed so far. On the basis of the present study we recommend that the optical properties (size, shape, and refractive index) of letovicite and the morphology of mixed-phase particles containing letovicite and a remaining liquid should be investigated in order to understand the influence of these mixtures on the radiative balance.

As a final conclusion of the present work and the global aerosol physical state modeling study[6] three major implications result: (i) Crystalline ammoniated sulfate particles, especially letovicite, are very likely to occur throughout the whole atmosphere. (ii) These aerosols are not expected to be pure solids but mixtures of one or more solids and a remaining liquid. (iii) The morphologies of these aerosols are probably very diverse and complex and, hence, not easily predictable.

Acknowledgment. The authors thank T. Koop, K. S. Carslaw, and B. P. Luo for discussing experimental data. C.A.C. thanks K. S. Carslaw for introducing her to thermodynamic models and providing the basic draft of Figure 2. Thanks are also given to Y. Kriescher for providing some additional experimental data. We acknowledge internal funding by the Swiss Federal Institute of Technology (ETH).

References and Notes

(1) *Intergovernmental Panel on Climate Change (IPCC): Third Assessment Report: Climate Change 2001*; WMO/UNEP; Cambridge University Press: 2001.
(2) Liou, K. N. *Mon. Weather Rev.* **1986**, *114*, 1167−1197.
(3) Ström, J.; Strauss, B.; Anderson, T.; Schröder, F.; Heintzenberg, J.; Wendling, P. *J. Atmos. Sci.* **1997**, *54*, 2542−2553.
(4) Seinfeld, J. H. *Nature* **1998**, *391*, 837.
(5) DeMott, P.; Lynch, D. K.; Sassen, K.; Starr, D. *Cirrus*; Oxford University Press: London, 2001.
(6) Colberg, C. A.; Luo, B. P.; Wernli, H.; Koop, T.; Peter, Th. *Atmos. Chem. Phys. Discuss*. **2002**, *2*, 2449−2487.
(7) Weis, D. D.; Ewing, G. E. *J. Geophys. Res.* **1999**, *104*, 21275−21285.
(8) Cheng, R. J.; Blanchard, D. C.; Cipriano, R. *Atmos. Res.* **1988**, *22*, 15−25.
(9) Ebert, M. Ph.D. Dissertation, TU Darmstadt, Fachbereich Chemie, 2000. http://elib.tu-darmstadt.de/diss/000047/.
(10) Pinnick, R. G.; Auvermann, H. J. *J. Aerosol Sci.* **1979**, *10*, 55−74.
(11) Braun, C.; Krieger, U. K. *Opt. Express* **2001**, *8*, 314−321.
(12) Kolb, C. E.; Worsnop, D. R.; Zahniser, M. S.; Davidovids, P.; Keyser, L. F.; Leu, M.-T.; Molina, M. J.; Hanson, D. R.; Ravishankara, A. R. *Adv. Ser. Phys. Chem.* **1995**, *3*, 771−875.
(13) Li, S. M.; Macdonald, M.; Strapp, J. W. *J. Geophys. Res.* **1997**, *102*, 21341−21353.
(14) Talbot, R. W.; Dibb, J. E.; Loomis, M. B. *J. Geophys. Res.* **1998**, *25*, 1367−1370.
(15) Dibb, J. E.; Talbot, R. W.; Scheuer, E. M.; Blake D. R.; Blake, N. J.; Gregory, G. L.; Sachse, G. W.; Thornton, D. C. *J. Geophys. Res.* **1999**, *104*, 5785−5800.
(16) Chow, J. C.; Watson, J. G.; Edgerton, S. A.; Vega, E. *Sci. Total Environ.* **1999**, *26*, 2391−2394.
(17) Liu, D. Y.; Prather, K. A.; Hering, S. V. *Aerosol Sci. Technol.* **2000**, *33*, 71−86.
(18) Tabazadeh, A.; Toon, O. B. *Geophys. Res. Lett.* **1998**, *25*, 1379−1382.
(19) Martin, S. T. *Geophys. Res. Lett.* **1998**, *25*, 1657−1660.
(20) Murphy, D. M.; Thomson, D. S.; Mahoney, T. M. J. *Science* **1998**, *282*, 1664−1669.
(21) Seinfeld, J. H.; Pandis, S. N. *Atmospheric chemistry and Physics*; John Wiley and Sons Inc.: New York, 1998.
(22) Noble, C. A.; Prather, K. A. *Environ. Sci. Technol.* **1996,** *30*, 2667−2680.
(23) Held, A.; Hinz, K. P.; Trimborn, A.; Spengler, B.; Klemm, O. *J. Atmos. Sci.* **2002**, *33*, 581−594.
(24) Martin, S. T. *Chem. Rev.* **2000**, *100*, 3403−3453.
(25) Clegg, S.; Brimblecombe, P.; Wexler, A. S. *J. Phys. Chem*. A **1998**, *102*, 2127−2154 http://www.hpc1.uea.ac.uk/~e770/aim.html.
(26) Zondlo, M. A.; Hudson P. K.; Prenni A. J.; Tolbert, M. A. *Annu. Rev. Phys. Chem.* **2000**, *51*, 473−499.
(27) Gable, C. M.; Betz, H. F.; Maron, S. H. *J. Am. Chem. Soc.* **1950**, *72*, 1445.
(28) Seidell, A. *Solubilities of Inorganic and Organic Compounds*; Norstrand: New York, 1940.
(29) Wexler, A. S.; Seinfeld, J. H. *Atmos. Environ.* **1991**, *25A*, 2731−2748.
(30) Richardson, C. B.; Spann J. F. *J. Aerosol Sci.* **1984**, *15*, 563−571.
(31) Tang, I. N.; Munkelwitz H. R.; Davis, J. G. *J. Aerosol Sci.* **1978**, *9*, 505−511.
(32) Spann, J. F.; Richardson, C. B. *Atmos. Environ.* **1985**, *19*, 819−825.
(33) Tang, I. N.; Munkelwitz, H. R. *J. Geophys. Res.* **1994**, *99*, 18801−18808.
(34) Martin, S. T.; Schlenker, J. C.; Malinowski, A.; Hung, H. M.; Rudich, Y. *Geophys. Res. Lett.* **2003**, *30* (21), 2102 doi: 10.1029/2003GL017930.
(35) Chelf, H. J.; Martin, S. T. *Geophys. Res. Lett.* **1999**, *26*, 2391−2394.
(36) Koop, T.; Bertram, A. K.; Molina, L. T.; Molina, M. J. *J. Phys. Chem. A* **1999**, *103*, 9042−9048.
(37) Yao, Y.; Massucci, M.; Clegg, S. L.; Brimblecombe, P. *J. Phys. Chem. A* **1999**, *103*, 3678−3686.
(38) Imre, D. G.; Xu J.; Tang, I. N.; McGraw, R. *J. Phys. Chem. A* **1997**, *101*, 4191−4195.
(39) Xu, J.; Imre, D.; McGraw, R.; Tang, I. *J. Phys. Chem. B* **1998**, *102*, 7462−7469.
(40) Onasch, T. B.; Siefert, R. L.; Brooks, S. D.; Prenni, A. J.; Murray, B.; Wilson, M. A.; Tolbert, M. A. *J. Geophys. Res.* **1999**, *104*, 21317−21326.
(41) Cziczo, D. J.; Abbatt, J. P. D. *J. Geophys. Res.* **1999**, *104*, 13781−13790.
(42) Bertram, A. K.; Koop, T.; Molina, L. T.; Molina, M. J. *J. Phys. Chem. A* **2000,** *104*, 584−588, 2000.
(43) Chen, Y. L.; DeMott, P. J.; Kreidenweis, S. M.; Rogers, D. C.; Sherman, D. E. *J. Atmos. Sci.* **2000**, *57*, 3752−3766.
(44) Prenni, A. J.; Siefert, R. L.; Onasch, T. B.; Tolbert, M. A.; DeMott, P. J. *Aerosol Sci. Technol.* **2000**, *32*, 465−481.
(45) Chelf, J. H.; Martin, S. T. *J. Geophys. Res.* **2001**, *106*, 1215−1226.
(46) Han, J. H.; Martin, S. T. *J. Geophys. Res.* **1999**, *104*, 3543−3553.
(47) Onasch, T. B., McGraw, R.; Imre, D. *J. Phys. Chem.* **2000**, *104*, 10797−10806.
(48) Koop, T.; Luo, B. P.; Biermann, U. M.; Crutzen, P. J.; Peter, Th. *J. Phys. Chem.* **1997**, *101*, 1117−1133.
(49) Colberg, C. A. Ph.D. Dissertation, ETH Zürich, 2001. http://e-collection.ethbib.ethz.ch/cgi-bin/show.pl?type=diss&nr=14331.
(50) Davies, E. J.; Buehler, M. F.; Ward, T. L. *Rev. Sci. Instrum.* **1990**, *61*, 1281−1288.
(51) Richardson, C. B. *Rev. Sci. Instrum.* **1990**, *61*, 1334−1335.
(52) Davies, E. J.; Periasamy, R. *Langmuir* **1985**, *1*, 373−379.
(53) Gmelin, L. *Gmelins Handbuch der Anorganischen Chemie, Amonium, System Nummer 23*; Verlag Chemie GmbH; Berlin, 1936.
(54) Krieger, U. K.; Braun, C *J. Quant. Spectrosc. Radiat. Transfer* **2001**, *70*, 545−554.
(55) Krieger U. K.; Braun C.; Imbach, L.; Koop, T.; Corti, C.; Videen, G. *J. Quant. Spectrosc. Radiat. Transfer* **2003**, *79*−*80*, 873−880.
(56) Videen, G.; Pellegrino, P.; Ngo D.; Videen, J. S.; Pinnick, R. G. *Appl. Opt*. **1997**, *36*, 6115−6118.
(57) Colberg, C. A.; Krieger, K. U.; Knopf, D. A.; Peter, Th. Unpublished work, to be submitted for publication.
(58) Cziczo, D. J.; Abbatt, J. P. D. *J. Phys. Chem. A* **2000**, *104*, 2038−2047.
(59) Colberg, C. A.; Krieger, K. U.; Peter, Th. Unpublished work, to be submitted for publication.
(60) Gysel, M.; Weingartner, E.; Baltensperger, U. *Environ. Sci. Technol.* **2001**, *36*, 63−68.
(61) Hämeri, K.; Vakeva, M.; Hansson, H. C.; Laaksoonen, A. *J. Geophys. Res.* **2000**, *105*, 22231−22242.
(62) Leong, K. H. *J. Aerosol Sci.* **1987**, *18*, 511−524.
(63) Cziczo D. J.; Nowak, J. B.; Hu, J. H.; Abbatt, J. P. D. *J. Geophys. Res.* **1997**, *102*, 18843−18850.
(64) Zuberi, B.; Bertram, A. K.; Koop, T.; Molina, L. T.; Molina, M. J. *J. Phys. Chem. A* **2001**, *105*, 6458−6464.
(65) Finlayson-Pitts, B. J.; Hemminger, J. C. *J. Phys. Chem. A.* **2000**, *104*, 11463−11477.
(66) Knipping, E. M.; Lakin, M. J.; Foster, K. L.; Jungwirth, P.; Tobias, D. J.; Gerber, R. B.; Dabdub, D.; Finlayson-Pitts, B. J. *Science* **2000**, *288*, 301−306.
(67) Cohen, M. D.; Flagan, R. C.; Seinfeld, J. H. *J. Phys. Chem.* **1987**, *91*, 4563−4574.
(68) Cohen, M. D.; Flagan, R. C.; Seinfeld, J. H. *J. Phys. Chem.* **1987**, *91*, 4583−4590.